Chinese Journal of Polymer Science Vol. 35, No. 8, (2017), 909–923

Chinese Journal of Polymer Science
© Chinese Chemical Society
Institute of Chemistry, CAS
Springer-Verlag Berlin Heidelberg 2017

Effect of Trastuzumab on the Micellization Properties, Endocytic Pathways and Antitumor Activities of Polyurethane-based Drug Delivery System*

Ni-jia Song[a†], Li-juan Zhou[a, b†], Wen-kai Liu[a], Xue-ling He[a, c], Zhi-cheng Pan[a], Ming-ming Ding[a], Xin-yuan Wan[a], Jie-hua Li[a**], Hong Tan[a**], Feng Luo[a] and Qiang Fu[a]

[a] *College of Polymer Science and Engineering, State Key Laboratory of Polymer Materials Engineering, Sichuan University, Chengdu 610065, China*

[b] *Key Laboratory of Rubber-Plastics, Ministry of Education/Shandong Provincial Key Laboratory of Rubber-Plastics, Qingdao University of Science & Technology, Qingdao 266042, China*

[c] *Laboratory Animal Center of Sichuan University, Huaxi Clinical College, Sichuan University, Chengdu 610040, China*

Abstract Polyurethane micelles (PM)-based nanovehicles have shown great potential in targeted delivery of therapeutics and diagnostics into tumors. However, the pathways of PMs entering cancer cells and the action mechanism of targeting ligands have yet to be understood. In this contribution, the actively-targeted PM were developed using trastuzumab as a model targeting group. It was found that PM were mainly taken up by SKOV-3 tumor cells *via* a micropinocytosis process, while the incorporation of trastuzumab to PM enabled a receptor-mediated endocytosis of nanocarriers in cancer cells, leading to more efficient cell entry and enhanced anticancer efficacy of chemotherapeutic drugs both *in vitro* and *in vivo*. This study is advantageous to the understanding of the action mechanism of trastuzumab, and significant for the construction of improved formulations for targeted delivery and precise therapy.

Keywords Polyurethane; Micelle; Trastuzumab; Endocytic pathway; Antitumor

INTRODUCTION

To address the challenges posed by the complexity, diversity and dynamic nature of cancer, many engineering tools and techniques have been developed and used in the anticancer treatment[1–5]. Chemotherapy has been the most common treatment for cancer, but it still faces some tremendous challenges: serious systemic side effects, multidrug resistance (MDR) and the deadly metastasis of cancer cells. Immunotherapy, using the human immune system to treat tumors, has great potential to solve or avoid the problems of chemotherapy. Moreover, it is reported that the combination of cancer immunotherapy or chemotherapy and biomaterial-based delivery system (BDS) appears more effective[6–8], for BDS has many functions such as targeted delivery to activate immune cells[9], synergy therapy of chemotherapy and cancer vaccines[10], and amplified immune activation by the stimuli-responsiveness or inherent immunostimulation of the materials[11]. In addition, BDS is expected to display desired functions with minimized negative side effects[12, 13]. To further explore the potential of BDS for

* This work was financially supported by the National Natural Science Foundation of China (Nos. 51273126 and 51573112), the National Science Fund for Distinguished Young Scholars of China (No. 51425305) and the Youth Science and Technology Innovation Team of Sichuan Province (No. 2015TD0001).

** Corresponding authors: Jie-hua Li (李洁华), E-mail: jiehua_li@scu.edu.cn
Hong Tan (谭鸿), E-mail: hongtan@scu.edu.cn

† These authors contributed equally to this work.

Received February 12, 2017; Revised March 13, 2017; Accepted March 13, 2017
doi: 10.1007/s10118-017-1952-3

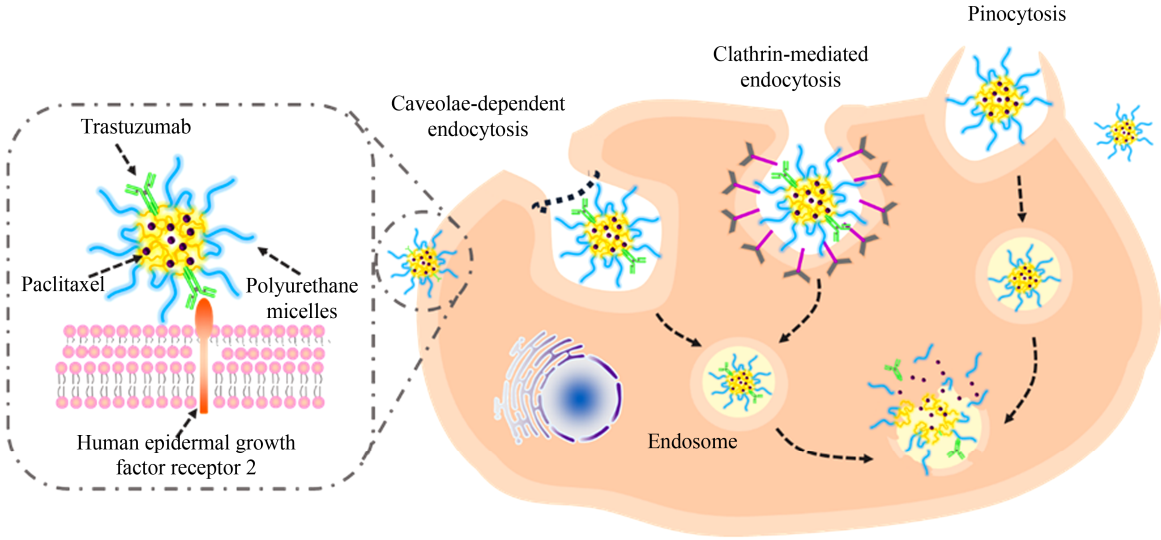
overcoming the complicated physiological barriers, considerable efforts have been made to exploit BDS equipped with multiple functions, such as prolonged circulation in the blood[14, 15], active targeting ability[16, 17], responsiveness to local stimuli[18–20], effective intracellular delivery[21, 22] and controlled release[23, 24].

Targeting ability is a crucial requirement for BDS, since it can improve the accumulation of drug formulations into tumor sites and increase the drug bioavailability and specificity[21, 25]. To this end, BDS has been bioengineered with a variety of synthetic and natural compounds to enhance its interactions with tumor cells and promote the cell internalization[26]. The frequently used targeted moieties including proteins (antibodies and their fragments)[27, 28] , nucleic acids (aptamers)[29, 30], and other small molecules (peptides, vitamins, and carbohydrates)[31, 32] have been shown to target the receptors overexpressed on the cancer cell surface, and assist in cell entry by receptor-mediated endocytosis. As an important humanized monoclonal antibody, trastuzumab can bind to the extracellular domain of human epidermal growth factor receptor 2 (HER2), and inhibit the proliferation of HER2-dependent cancer cells and even induce the cell apoptosis[33–36]. HER2 is highly expressed in different types of solid tumors such as breast cancer, ovarian cancer, and gastric cancer[36], while in normal tissues, it is presented at low levels and only in certain types of epithelial cells[37]. Therefore, the overexpression of HER2 endows trastuzumab with high selectivity in tumor cells, and accordingly may enhance the interaction of tumor cells and BDS conjugated with trastuzumab as a targeting ligand[38–40].

As targeted BDS can interact actively and selectively with tumor cells, it is more desirable that the nanoparticles enter cells rapidly. Given the size of BDS commonly used for delivery purpose (10–200 nm), most of the BDS is taken up by cells through micropinocytosis, a kind of active cell physiological process[21, 41]. Another important pathway of BDS coupled with targeting molecule is receptor-mediated internalization, which occurs mainly through clathrin-dependent endocytosis or caveolin-dependent endocytosis[21, 41]. Moreover, it is demonstrated that the disparate endocytosis pathways have great effects on the degree of cellular uptake. For example, Hu *et al*. have found that the nanocarriers with staggered lamellae nanostructures display the fastest cellular uptake rates mainly by clathrin- and caveolae-independent endocytosis compared to other nanocarriers with other types of nanostructures including spheres and smooth disks which mainly follow clathrin- and caveolae-endocytosis[42]. Although trastuzumab is widely used to improve the targeting capacity of BDS toward HER2-overexpressing breast cancers, its mechanism of action is not fully understood[43]. Initial studies proposed that trastuzumab may downregulate HER2 through receptor-mediated endocytosis and lysosomal degradation[44–46]. However, recent clinical data suggest that this assumption is conflicting[46, 47]. Hommelgaard *et al*. found HER2 an internalization-resistant receptor because of the preferential association of HER2 with plasma membrane protrusions[47], while using the same tumor cell line, Cuello *et al.* reported that trastuzumab could downregulate the HER2 protein[45]. Therefore, the study on whether trastuzumab can mediate the endocytosis of BDS after binding to HER2 is not only beneficial to the understanding of the action mechanism of trastuzumab, but also significant for the development of improved formulations for targeted delivery and precise therapy.

In this study, we develop a pH sensitive polyurethane micelle (PM) conjugated with trastuzumab as a targeting group, and investigate the impact of antibody on the properties of the BDS in detail (Scheme 1). BDS based on polyurethane has shown great potential in targeted delivery of therapeutics and diagnostics into tumors[48–53]. As demonstrated previously by our group, polyurethane micelles bearing antibodies and folate can ferry chemotherapy drugs selectively into tumors both *in vitro* and *in vivo*, and remarkably improve the biodistribution and antitumor efficacy[48–51]. However, the pathways of polyurethane micelles entering tumor cells and the action mechanism of the targeting ligands have yet to be understood. In this contribution, we use trastuzumab as a targeting ligand, and carefully track the endocytic pathways of the PM and trastuzumab-modified PMs. The detailed cellular uptake mechanism was evaluated with flow cytometry and confocal laser scanning microscopy (CLSM). These data illustrate that PM are mainly internalized *via* micropinocytosis, while the uptake of trastuzumab-conjugated TPM by SKOV-3 cells primarily occurred *via* a clathrin-mediated endocytosis (Scheme 1). To test the therapeutic efficiency of the targeted PM (TPM), paclitaxel (PTX) was

encapsulated as a model drug, and the antitumor activity against SKOV-3 tumor cells was assessed both *in vitro* and *in vivo*.



Scheme 1 Schematic of the construction and the endocytic pathway of targeted polyurethane micelles (TPM)
The pH sensitive polyurethane micelle (PM) conjugated with trastuzumab can bind to cells overexpressing extracellular domain of human epidermal growth factor receptor 2 (HER2). PM are mainly internalized *via* micropinocytosis, while the uptake of trastuzumab-conjugated TPM by SKOV-3 cells primarily occurred *via* a clathrin-mediated endocytosis.

EXPERIMENTAL

Materials

Paclitaxel (PTX, 99.5%, Jinhe Bio-Technology Co., Ltd., China), *N*-hydroxy succinimide (HOSu, ≥ 98%, Alfa Aesar, USA) and 1-[3-(dimethylamino) propyl]-3-ethylcarbodiimide methiodide (EDC·HCl, 98.0%, J&K Chemical Ltd., China) were used without purification. Fluorescein isothiocyanate isomer I (FITC, 90%) was from Acros Organics (USA). Trastuzumab was purchased from Roche (Basel, Switzerland) and stored at 4 °C until use, and 4-(2-hydroxyethyl)-1-piperazine-ethanesulfonic acid (HEPES) was purchased from Invitrogen (Carlsbad, USA). Taxol was commercially available from West China Hospital, Sichuan University, China. All the other chemicals were reagent grade. The pH sensitive polyurethanes were prepared according to our previous work[54].

Characterization

Size and zeta potentials of TPM and PM were measured with a Zetasizer Nano ZS DLS instrument (Malvern Instruments, Malvern, UK) at 25 °C and an angle of 90°. Data for each sample were obtained in three parallel measurements.

Transmission electron microscopy (TEM, model H-600-4, Hitachi, Tokyo, Japan) was performed at an accelerating voltage of 75 kV. A drop of micellar solution stained with 0.01 g/mL phosphotungstic acid was placed on a copper grid with Formvar film, and the liquid was blotted off and the grid was air-dried before measurements.

Preparation of TPM

PM were prepared using a modified dialysis method. The synthetic polyurethanes (25 mg) dissolved in 5 mL of dimethylacetamide (DMAc) were added dropwise to 15 mL of deionized water with vigorous magnetic stirring. The mixed solution was dialyzed against deionized water in a dialysis tube (molecular weight cut-off, MWCO 3500) for about 3 days at room temperature to remove the organic solvent. The micelle solution was centrifugalized at 3000 r/min for 20 min and passed through a 0.45 μm pore size syringe filter (Millipore,

Carrigtwohill, Co. Cork, Ireland). The prepared micelles are named as PM.

To generate actively targeted TPM, the monoclonal antibody trastuzumab was conjugated to PM *via* the carboxyl groups of the tripeptide side chains, which was introduced into the polyurethane as chain extender[54]. Briefly, 5 mL of the PM solution (1 mg/mL) was mixed with 1 mL of HEPES-buffered saline (pH 7.0) for 30 min. Then EDC·HCl (6.2 μL, 0.25 mol/L) and HOSu (9.3 μL, 0.25 mol/L) were added, and the mixture was incubated for 1 h at room temperature. The pH of the solution was adjusted to 7.5 with 1 mol/L NaOH, and 25 μL of trastuzumab (1 mg/mL in PBS) was added and incubated for 8 h at room temperature with gentle stirring. When the reaction was completed, free antibody was removed by dialyzing against phosphate buffered saline (PBS, pH 7.4) and the precipitate was removed using a 0.45 μm pore size syringe filter. The amount of grafted antibody was confirmed by an enzyme-linked immunosorbent assay (ELISA).

Enzyme-linked Immunosorbent Assay

ELISA was performed to confirm the successful conjugation of trastuzumab to PM and measure the amount of grafted antibody as described below. The solution of lyophilized samples re-dissolved in Na_2CO_3 buffer (0.05 mol/L) was added into 96-well plates (100 μL/well) and kept at 4 °C overnight, then washed with PBS containing 0.1% Tween-20 and 0.05% NaN_3 (PBS/Tween/azide), followed by a single wash with PBS/azide. Afterwards, the plates were incubated with a blocking buffer containing 2% bovine serum albumin (BSA) in PBS/Tween/azide for 2 h and washed again as above process. Thereafter, a horseradish peroxidase (HRP)-conjugated anti-trastuzumab (secondary antibody, 5 μg/mL) was added into each well. The plates were incubated at 37 °C for 1 h and washed as above. Coloration was initiated by treating with *o*-phenylenediamine (OPD, Sigma, St. Louis, MO) for 30 min at 37 °C in the dark and stopped by 50 μL of 2 mol/L H_2SO_4. The optical density (OD) was measured at 492 nm by a microplate reader (Model 680, Bio Rad Corp.). The spectrophotometer was calibrated with standard 0.5 ng/mL to 800 ng/mL trastuzumab solutions. Solutions of unconjugated micelles served as the blank. The concentration of trastuzumab in the micelles was determined by optical density against the standard curve, and calculated as the weight of antibody (micrograms antibody) associated with unit weight (milligrams) of lyophilized PM. Standard equation extrapolated from the standard curve is listed as follows:

$$\text{Antibody concentration} = 15460.04111 \times OD^2 + 62.84282 \times OD - 96.33645$$

Drug Loading Capacity

PTX was loaded by a micelle extraction technique. Briefly, a certain amount of PTX stock solution in acetone was added to empty vials and evaporated by nitrogen, then the micelle solution was transferred into the vials and ultrasonicated for 2 h. The solution was centrifuged and filtered to get PTX-loaded micelles (TPM-PTX and PM-PTX). The PTX concentration was detected by Agilent 1260 Infinity high-performance liquid chromatography (HPLC) system (Agilent Technologies Inc., USA). The flow rate was 1.0 mL/min, and the mobile phase consisted of acetonitrile/water (60/40, *V*/*V*). The detection of PTX was performed by UV absorption at 227 nm. Drug loading content (LC) and encapsulation efficiency (EE) were calculated with the following equations:

$$\text{Drug loading content (\%)} = \frac{\text{weight of DOX in the micelles}}{\text{weight of DOX} - \text{loading micelles}} \times 100$$

$$\text{Encapsulation efficiency (\%)} = \frac{\text{the amount of DOX in micelles}}{\text{the amount of DOX feeding}} \times 100$$

The FITC loaded micelles were prepared in the same way.

Cell Culture

Human ovarian cancer SKOV-3 cells were purchased from West China Medical Center of Sichuan University (Sichuan, China) and maintained in Roswell Park Memorial Institute 1640 medium (HyClone Laboratories Inc., Logan, UT, USA) containing 10% fetal bovine serum and 5% penicillin-streptomycin (both from Life Technologies, Carlsbad, CA, USA) in a humidified atmosphere of 5% CO_2 at 37 °C.

Flow Cytometry

SKOV-3 cells were seeded into six-well flasks (Corning, USA) at a density of 5×10^5 cells/well and cultured at 37 °C overnight. These cells were washed with PBS (pH 7.4) three times to remove the remnant growth medium, and incubated with micelle samples in serum-free medium for scheduled time. Afterwards, the medium was sucked away and the cells were washed thrice with PBS. Finally, the cells were collected *via* detaching by 0.25 g/mL trypsin, centrifugation and suspending in 0.5 mL of PBS. The degree of cellular uptake was analyzed based on the FITC fluorescence using a FACS Aria flow cytometer (BD Biosciences). The FITC loaded micelles were prepared in the same way as PTX-loaded micelles.

Confocal Laser Scanning Microscope (CLSM)

SKOV-3 cells were seeded in six-well plates (a clean coverslip was put in each well, 24 mm × 24 mm) at a density of 1×10^5 cells/well and cultured at 37 °C overnight. The cells were then incubated with micelle samples for different time. After the supernatant was removed, these cells were washed three times with cold PBS, fixed by 1 mL of 4% paraformaldehyde for 30 min at 4 °C, and then stained with 2-(4-amidinophenyl)-6-indolecarbamidine dihydrochloride (DAPI, 10 μg/mL, Sigma-Aldrich, USA) for 10 min. The slides were mounted with 50% glycerol solution and examined using a Leica TCS SP5 (Leica Microscopy Systems Ltd., Germany). The FITC loaded micelles were prepared in the same way as PTX-loaded micelles.

Investigation of Endocytic Pathway

SKOV-3 cells (1×10^5 cells/well) were separately seeded in 6-well plates with 2 mL of RPMI 1640 media and incubated for 24 h. To evaluate the endocytic pathway of PM and TPM, the cells were pretreated individually with three different inhibitors of endocytosis for 30 min at 37 °C. The inhibitors selected were chlorpromazine (CPZ, 10 μg/mL) to inhibit the clathrin-mediated endocytosis, genistein (Geni, 20 μg/mL) to inhibit caveolae-mediated endocytosis, and amiloride (Amil, 10 μg/mL) to inhibit micropinocytosis. All the inhibitors were used at nontoxic concentrations according to the results of other publications in order to achieve a minimum of 90% cell viability[55, 56]. Following the pretreatment, 1 mL of TPM and PM loaded FITC were added, and the plates were incubated for another 2 h. The cells incubated with FITC-loaded micelles without any chemical inhibitor pretreatment were used as controls. Subsequently, the cells were washed three times with PBS and fixed with 4% paraformaldehyde for 30 min, and the cell nuclei were stained with DAPI for 10 min. The fluorescence images were observed using CLSM. For quantitative analysis, the cells were washed three times with PBS and were manipulated in a similar manner to that used in flow cytometry, as described above.

Cellular Uptake

The cellular uptake of FITC-loaded micelles with or without trastuzumab was studied by fluorescence detection. Cells were incubated with various FITC-loaded PM and TPM in serum-free medium for 0.5 and 1 h. The fluorescence images were observed using CLSM. For quantitative analysis, the cells were washed three times with PBS and manipulated in a similar manner to that used in flow cytometry, as described above.

Cytotoxicity Assay

The antitumor activity of PTX-loaded micelles *in vitro* was evaluated by an MTT assay. SKOV-3 cells were seeded in 96-well plates (Corning) (5×10^3 cells/well) and incubated at 37 °C for 24 h. The cells were treated with 100 μL of medium containing various concentrations of drug-free and PTX-loaded micelles. The culture medium and Taxol solutions diluted to the same concentrations were set as negative and positive controls, respectively. At the designated time intervals (24 and 72 h), 20 μL of MTT solution in PBS (5 mg/mL, Sigma) was added to each well for 4 h of incubation at 37 °C. The culture medium was then discarded and the insoluble formazan crystals were dissolved in 100 μL of dimethyl sulfoxide. Plates were agitated on a shaker for 10 min, and the absorbance was measured at 490 nm on a microplate reader (DNM-9602, Perlove Medical Equipment Co., Ltd., Nanjing, China). Cell viability was calculated with the following equation:

$$\text{Cell viability (\%)} = \frac{\overline{\text{OD}}_{\text{Sample}}}{\overline{\text{OD}}_{\text{Control}}} \times 100$$

where $\overline{OD}_{Sample}$ and $\overline{OD}_{Control}$ are optical density values in wells containing micelle samples and culture medium, respectively. Cell viability (%) was plotted as a function of logarithmic PTX concentration and normalized to the value for untreated cells. Dose-response curves were generated and the median inhibitory concentration (IC_{50}) was determined using GraphPad Prism 5 for Windows software (GraphPad Software, Inc., San Diego, CA, USA). The analysis method chosen in this software is named "lg(inhibitor) versus normalized response—Variable slope". Data are presented as mean ± standard deviation.

Animals

The animal studies were carried out with the approval from the Ethics Committee of Sichuan University and in compliance with the Principles of Laboratory Animal Care of the National Institutes of Health, China. Female BALB/c mice (6–8 weeks) were purchased from the Laboratory Animal Center of Sichuan University (Sichuan, China). All the animals were kept under pathogen-free conditions according to AAALAC guidelines and were allowed to acclimatize for at least 4 days prior to any experiments.

In Vivo Antitumor Activity

To evaluate the antitumor effect of the TPM *in vivo*, the SKOV-3 tumor model was established by inoculation of 4×10^6 cells into the nude mice and the SKOV-3 tumor-bearing mice were randomly assigned to eight groups (n = 5). When the tumor size reached approximately 40 mm^3 in volume, Taxol at 6.0 mg/kg, TPM-PTX at 6.6 mg/kg, PM-PTX at 5.6 mg/kg and PBS as a control group were intravenously injected through the tail vein twice per week for 15 days. Targeted empty carriers (TPM) without drug loading were also administered at the same micellar dose and scheduled as the TPM-PTX formulations. The tumor volume was measured and calculated using the following formula: (width^2 × length)/2. The body weight and survival rate of each group were recorded for 17 days. Then mice were euthanized, and the tumors were separated, weighed, and sectioned for histological evaluation with hematoxylin and eosin (H&E) staining and analysis of the proliferating cell nuclear antigen (PCNA) for microscopic observation.

Statistics

Statistical analysis was performed using the Statistical Package for the Social Sciences (SPSS, version 17.0) software. Data are expressed as means ± standard deviations (SD). Student's t-test or one-way analysis of variance (ANOVA) at 95% confidence levels ($P < 0.05$) was conducted to assess statistical significance within the data.

RESULTS AND DISCUSSION

Preparation and Characterization of Polyurethane Micelles

The polyurethane micelles (PM) were prepared according to our previous work[54]. Trastuzumab, a humanized monoclonal antibody approved by Food and Drug Administration (FDA), was conjugated to the core-shell interface of PM. Trastuzumab has been widely used for the treatment of tumors that overexpress human epidermal growth factor receptor type 2 (HER2)[57, 58]. The grafting efficiency of trastuzumab is around 12%–15%, and the antibody content on the micelles is approximately 4 μg of antibody/mg micelles. As protein macromolecules, the trastuzumab incorporated may have impact on the properties of PM. Firstly, the average size of PM increases from 67.5 nm to 79.3 nm due to the huge volume of the antibodies (Fig. 1a). The polydispersity index of PM and TPM is 0.166 and 0.119, respectively. The particle size is in favor of tumor accumulation through an enhanced permeability and retention (EPR) effect[59]. Meanwhile, the TPM are regularly spherical and well-dispersed individual particles with narrow diameter distribution as observed by TEM (Fig. 1b), indicating that trastuzumab has no impact on the morphology of PM. Moreover, as the carboxyl groups on the polymer side chains are reacted with trastuzumab, the zeta potential of PM increases from −14.5 mV to −6.2 mV (Figs. 1c and 1d), which is conducive to the long circulation *in vivo*.

As one of the most potent anticancer drugs, PTX suffers from its poor solubility and acute toxicity to normal tissue, which greatly reduce the bioavailability and therapeutic efficiency. To evaluate the loading capacity of TPM as a vehicle for anticancer agents, PTX was chosen as a model hydrophobic drug. PTX was

loaded into the micelles using an extraction method. As illustrated in Fig. 2, the TPM can encapsulate PTX efficiently, with an encapsulation efficiency almost close to 80% and drug loading content up to 30%. The loading capacity of PM herein is quite higher than that of Genexol-PM, a polymeric micelle formulated paclitaxel approved by FDA. Moreover, TPM exhibit approximate drug loading efficiency compared with PM (Fig. 2), suggesting that the introduction of antibody does not affect the drug loading capacity of the micelles.

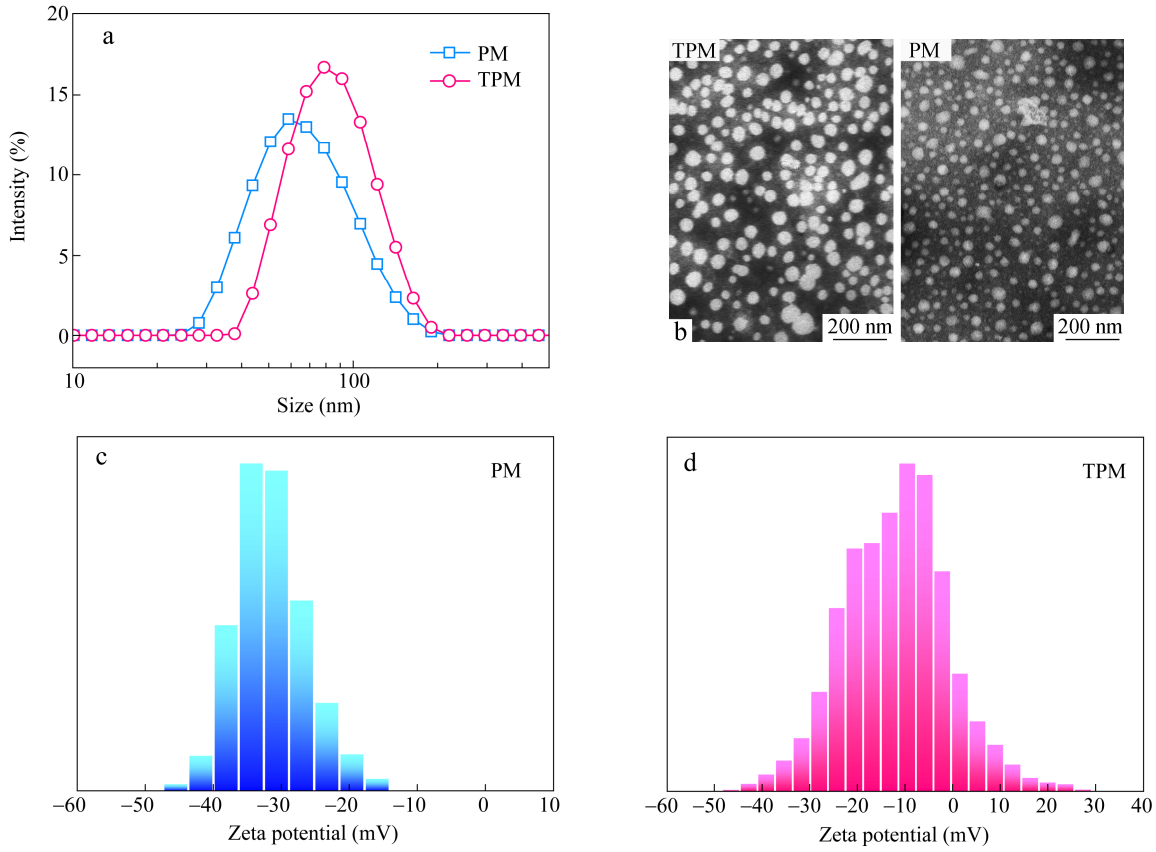


Fig. 1 (a) Size distribution, (b) TEM images and (c, d) zeta potential distribution of PM and TPM

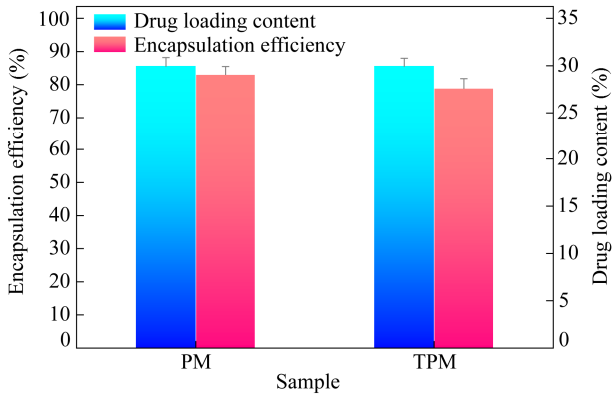


Fig. 2 Drug loading content and encapsulation efficiency of TPM and PM

The Endocytic Pathway

Trastuzumab can specifically bind to HER2, and is speculated to cause the internalization of the receptor-antibody combination by receptor-mediated endocytosis[45]. In this regard, trastuzumab may play an interesting

role in the cellular uptake pathways of PM. Normally, micelles self-assembled from macromolecules could be easily internalized *via* micropinocytosis[21, 41]. In particular, if the micelles interact with the receptors on the cytomembrane, a receptor-mediated internalization may occur through clathrin-dependent endocytosis or caveolin-dependent endocytosis[21, 41]. To investigate the endocytic pathway of PM and the action mechanism of trastuzumab, three inhibitors including chlorpromazine (CPZ), genistein (Geni), and amiloride (Amil) were employed to block the clathrin-mediated endocytosis[55, 56], caveolae-mediated endocytosis[60, 61], and macropinocytosis[60], respectively. Due to the over expressed HER2 receptors onto the surface, human ovarian carcinoma SKOV-3 cells were chosen as cell model *in vitro*[62, 63].

The cellular uptake was intuitively observed by CLSM (Fig. 3) and the integrated fluorescence intensity of each image was calculated by Image J (Fig. 4). For nontargeted micelles PM, as shown in Fig. 3, cells incubated with Amil exhibit much lower green fluorescence intensity than the control group, while those treated with CPZ display a slight decrease of fluorescence intensity. However, Geni has little impact on the uptake of PM. When

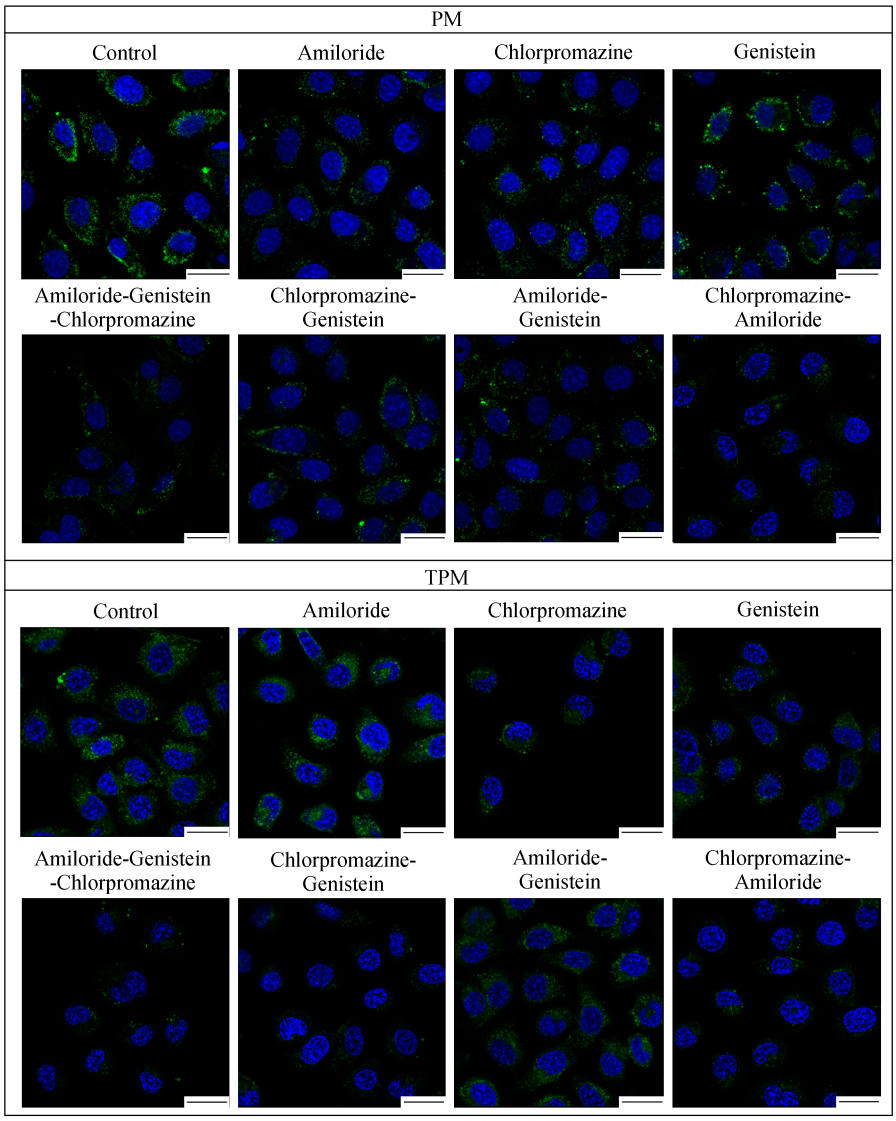


Fig. 3 CLSM images of SKOV-3 cells incubated with PM and TPM before and after the treatment with different endocytic inhibitors (Scale bar = 25 μm. The online version is colorful.)

treated with two inhibitors simultaneously, both groups receiving Amil demonstrate weak fluorescence intensity. These data illustrate that PM are mainly internalized *via* micropinocytosis. On the other hand, the uptake of trastuzumab-conjugated TPM by SKOV-3 cells primarily occurred *via* a clathrin-mediated endocytosis, for the fluorescence is declined significantly after this pathway was blocked by CPZ (Figs. 3 and 4). Moreover, the role of caveolae-mediated endocytosis pathways could not be ignored for the uptake of TPM by SKOV-3 cells (Fig. 3). As summarized in Fig. 4, there are huge differences between the endocytic pathways of PM and TPM. To better understand the cell entry, the internalization pathways of PM and TPM were further quantified by flow cytometry (Fig. 5). Obviously, the results are consistent with CLSM (Fig. 3), implying that PM is mainly internalized *via* a micropinocytosis process while the cellular uptake of TPM is through receptor-mediated endocytosis. These results confirm that the incorporation of antibody has a great impact on cellular internalization mechanism of polyurethane micelles by SKOV-3 cells. Accordingly, it can also be concluded that trastuzumab can mediate the endocytosis of polyurethane micelles after binding to HER2 receptor. In addition, after internalized through various endocytic routes, the BDS is invariably entrapped in endo-lysosomal compartments and confronted with the threat of degradation. Fortunately, we have recently demonstrated that the multifunctional polyurethane micelles can quickly escape from these acidic organelles mimicking the behavior of nonenveloped viruses, and effectively deliver drugs to cytoplasm[64]. Therefore, these molecular-engineered polyurethane systems hold great promise for specific intracellular and organelle delivery and precision medicine.

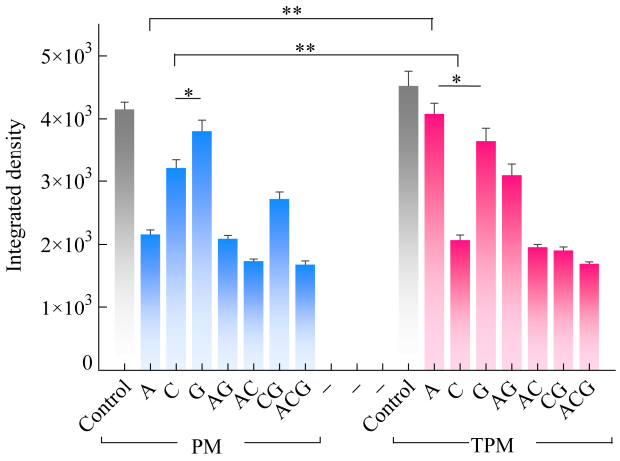


Fig. 4 Fluorescence intensity calculated from the CLSM images of SKOV-3 cells treated with different endocytic inhibitors
Three inhibitors, chlorpromazine (CPZ), genistein (Geni), and amiloride (Amil), are abbreviated as C, G and A, respectively. Statistical significance: (*) $P < 0.05$, (**) $P < 0.01$.

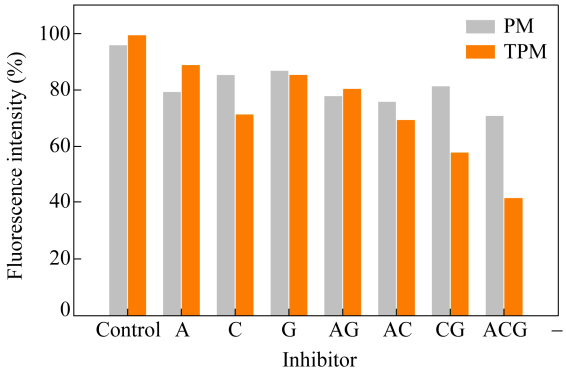


Fig. 5 Effect of added endocytic inhibitors on the internalization of PM and TPM to SKOV-3 cell as characterized by flow cytometry
Three inhibitors, chlorpromazine (CPZ), genistein (Geni), and amiloride (Amil), are abbreviated as C, G and A, respectively.

In Vitro Cellular Uptake

It has been proved above that trastuzumab can affect the endocytic pathway of PM, which may influence the interaction of micelles and cells and the extent of cell uptake of polyurethane micelles. To investigate the cellular uptake of TPM in SKOV-3 cells, flow cytometry and CLSM were carried out using fluorescein isothiocyanate (FITC) as a hydrophobic fluorescence probe (Fig. 6). As seen in Fig. 6(a), the relative intracellular FITC fluorescence intensity in SKOV-3 cells treated with TPM is significantly higher than that treated with PM over the same period, which proves that the micelles connected with antibodies have higher efficiency of cellular internalization. Furthermore, the cellular uptake was also quantized by flow cytometry analysis, and the result is in good agreement with CLSM (Fig. 6b), further confirming that the cellular uptake of TPM can be enhanced through the specific binding of trastuzumab and the HER2 receptors over expressed on the membrane of

SKOV-3. Further work is being carried out to investigate the different receptor-mediated endocytic paths on the intracellular trafficking of BDS.

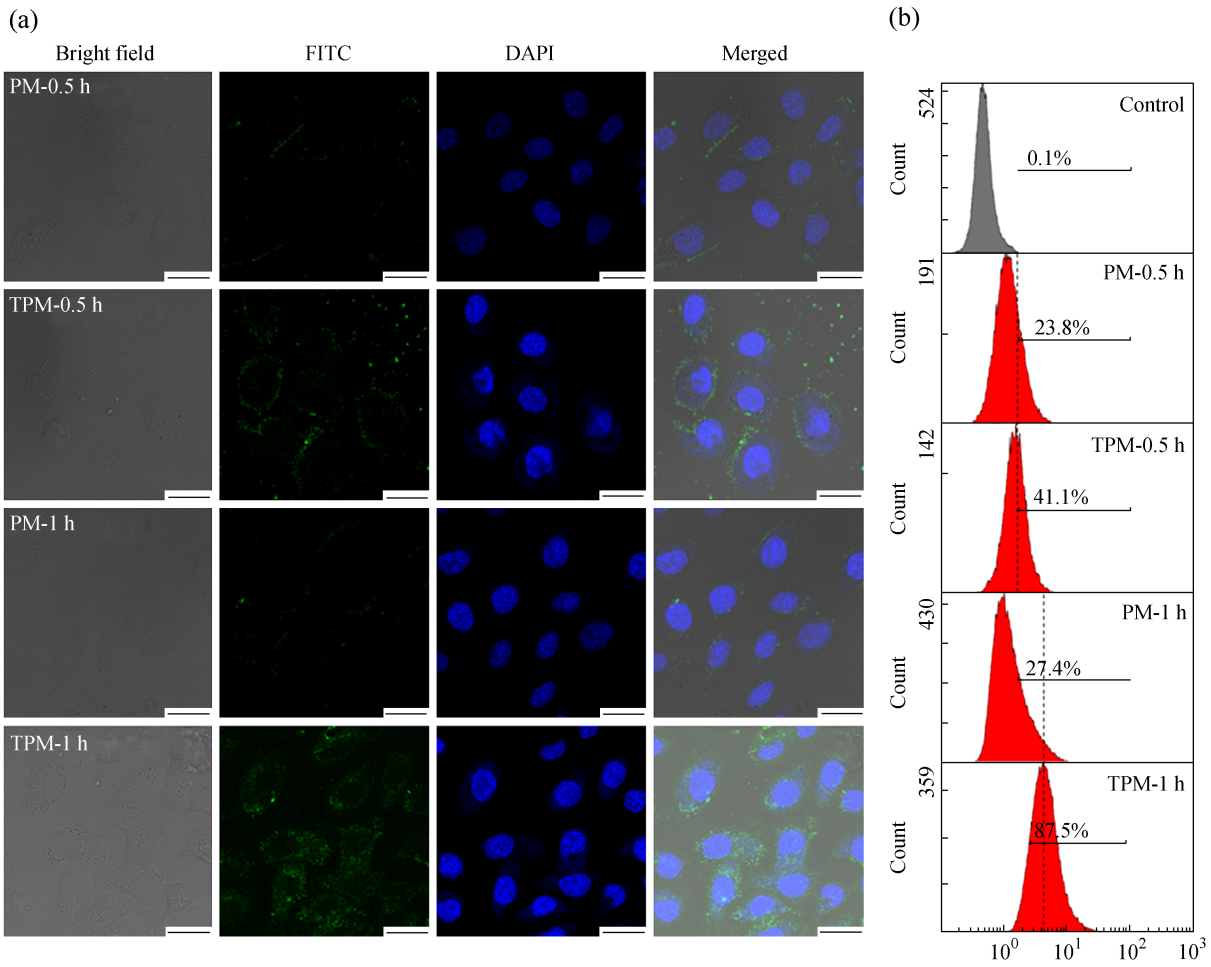


Fig. 6 (a) CLSM images of SKOV-3 cells incubated with FITC-loaded micelles with or without trastuzumab conjugation for different time (Nuclei of cells were stained with DAPI. Scale bar = 25 μm.); (b) Flow cytometry histogram profiles of SKOV-3 cells incubated with FITC-loaded micelles with or without trastuzumab for 0.5 and 1 h, respectively

In Vitro Antitumor Activity of TPM

MTT assay was carried out to assess the antitumorigenic potential of TPM against SKOV-3 cells. It was found that the cytotoxicity of the samples is dose-dependent. The IC_{50} was calculated to compare the cytotoxicity and illustrated in Fig. 7. Evidently, free paclitaxel shows the strongest toxicity, with IC_{50} values lower than those for micellar formulations, which is consistent with the results reported in some literatures[65, 66]. In addition, TPM demonstrate a higher cytotoxicity than nontargeted formulations, arising from its higher cellular uptake as observed by flow cytometry and CLSM. The IC_{50} of PTX-loaded TPM (9.32 μg/mL) is lower than that of PTX-loaded PM (15.00 μg/mL) after 72 h of incubation (Fig. 7c).

To exclude the possibility that micelles and antibody themselves are toxic to tumor cells, the viability of SKOV-3 cells incubated with drug-free micelles was also assessed (Fig. 8). The viability of blank micelles is greater than 90% after 24 and 72 h of incubation, indicating that TPM have no adverse effect on cell growth. Taken together, these results demonstrate that TPM are safe and effective for anticancer drug delivery.

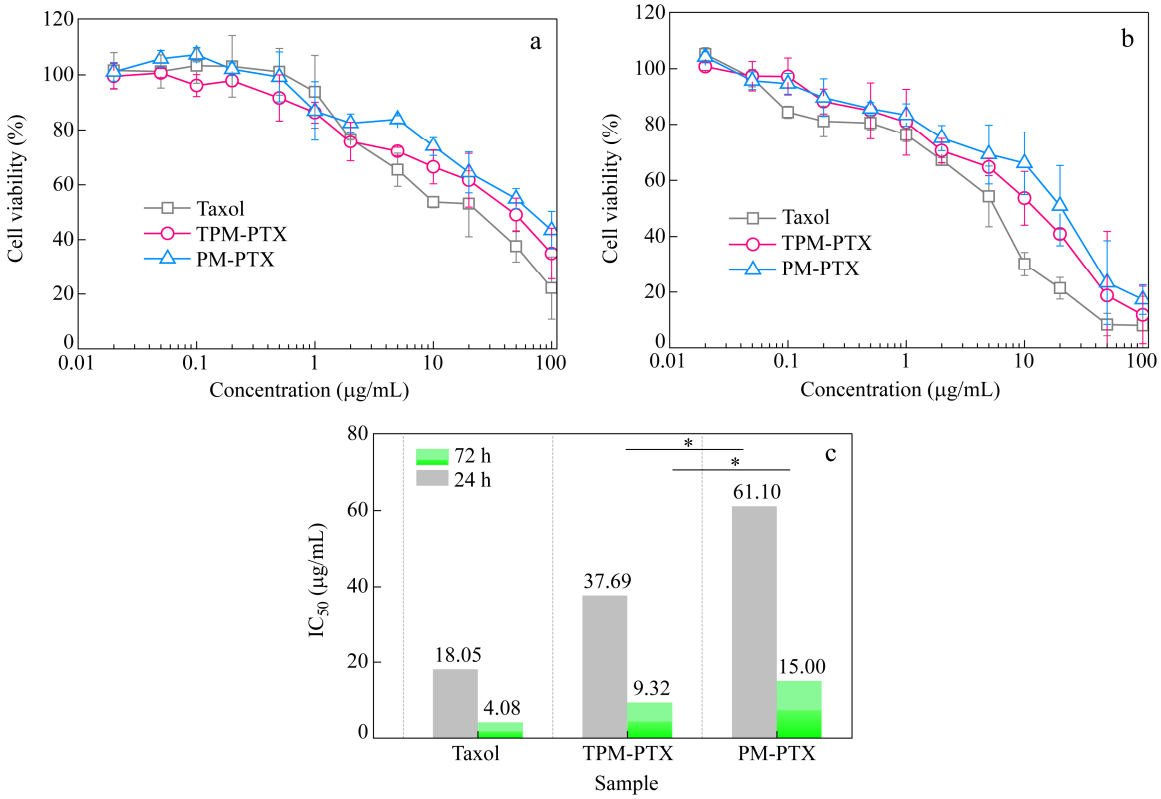


Fig. 7 Cell viability of SKOV-3 tumor cells after (a) 24 h and (b) 72 h of incubation with PTX-loaded PM; (c) The median inhibitory concentration (IC_{50}) of various PTX formulations for different incubation time (Statistical significance: (*) $P < 0.05$.)

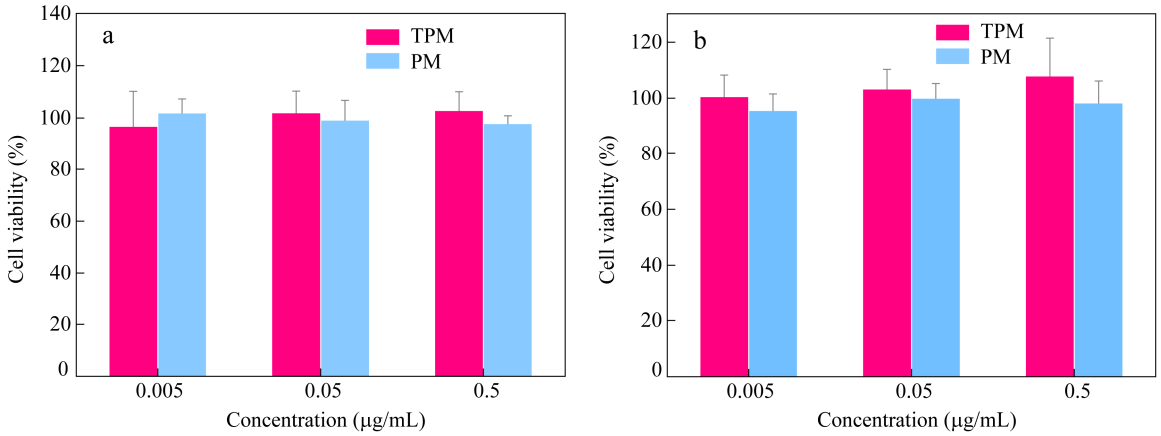


Fig. 8 Cell viability of SKOV-3 tumor cells after (a) 24 h and (b) 72 h of incubation with various concentrations of TPM and PM

In Vivo Antitumor Effect and Histological Analysis

To evaluate the *in vivo* therapeutic efficacy of PTX-loaded PM, various drug formulations were injected into SKOV-3 ovarian tumor-bearing nude mice *via* the tail vein. For comparison, commercial Taxol, drug-free PM and phosphate buffered saline (PBS, pH 7.4) were also administered as controls. No mice died during the treatment period and the body weight were essentially unchanged (Figs. 9a and 9d). It was found that the tumor planted in PBS-treated mice grow rapidly (Figs. 9b and 9c), while those receiving Taxol display moderate tumor

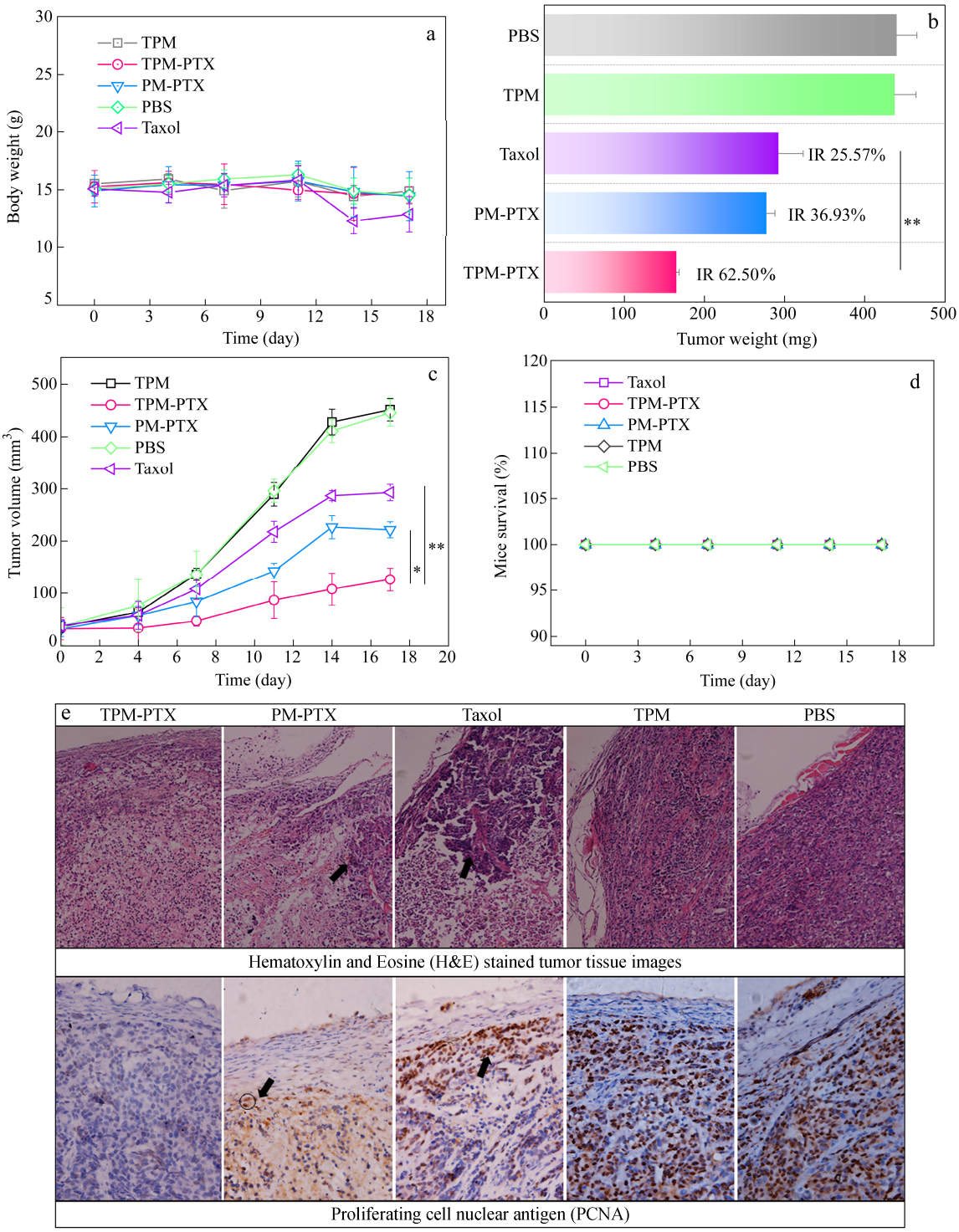


Fig. 9 (a) Body weight changes of animals measured and plotted as average; (b) Tumor weight and tumor growth inhibition rate (IR) calculated after excision; (c) Changes of tumor volume after injection of PM-PTX, targeted TPM-PTX, Taxol, blank micelles (TPM) and PBS in SKOV-3 ovarian tumor-bearing nude mice; (d) Survive rates of tumor-bearing mice receiving intravenous injection; (e) Hematoxylin and Eosine (H&E) stained tumor tissue images and analysis of proliferating cell nuclear antigen (PCNA) after therapy
Viable tissue and cells are pointed by black arrows in PM-PTX and Taxol. Statistical significance: (*) $P < 0.05$; (**) $P < 0.01$. The online version is colorful.

inhibition. On the other hand, the micellar formulations possess much higher antitumor activity than Taxol due to that the protection and targeting ability provided by PM result in greater accumulation of chemotherapeutic drugs in tumors (Figs. 9b and 9c). In particular, PTX-loaded PM exhibit varying tumor inhibition *in vivo* affected by their targeted groups. As shown in Fig. 9(c), the incorporation of trastuzumab antibody into polyurethane micelles significantly improves the antitumor activity of PM. The final tumor volume of TPM-PTX treated mice was 126.0 mm^3, which is 2-fold smaller than those treated with PM-PTX. Moreover, the tumor growth inhibition rates (IR) of PM-PTX and TPM-PTX are 36.93% and 62.50%, respectively (Fig. 9b). Though the trastuzumab can inhibit the proliferation of HER2-dependent cancer cells and even induce the cell apoptosis, the antibody content on the micelles is approximately 4 μg antibody/mg micelles as determined by an ELISA method (equivalent to 0.01 mg/kg body weight per dose), which is 2000-fold lower than that required for the treatment of tumor-bearing nude mice with free trastuzumab (20 mg/kg per dose)[67]. Furthermore, free TPM conjugated with trastuzumab as a control did not show any inhibition effect against SKOV-3 ovarian tumors *in vitro* (Fig. 8). Therefore, the enhanced therapeutic effect of targeted TPM-PTX versus untargeted one should be attributed to the antibody molecules that are specifically captured and anchored to the cell surface through an antibody-receptor interaction, allowing a rapid entry *via* receptor-mediated endocytosis mechanism, as we confirmed in this study. In addition, as shown in the histological analysis of tumor sections (Fig. 9e), severe damage is clearly observed in the tumor tissue of TPM-PTX treated mice. The necrotic tissues are quite sparse with many cavities. Similarly, from the analysis of the proliferating cell nuclear antigen (PCNA), apoptotic cells are stained purple, while cells with proliferative activity are brown. It was found that the cells in the tumor tissue from TPM-PTX-treated group almost lose their proliferative activity, while those from mice treated with PBS and blank micelles are quite vibrant. The superior therapeutic efficacy of TPM-PTX micelles is attributed to the higher amount of PTX reached cytoplasm of tumor cells, which results from trastuzumab-mediated endocytosis as well as the excellent endo-lysosomal escape capabilities of PM[64]. These results demonstrates that TPM are versatile vehicles for efficient tumor targeting and specific intracellular delivery of therapeutics.

CONCLUSIONS

In summary, we have successfully developed an actively-targeted polyurethane delivery system decorated with trastuzumab as a targeting ligand. The trastuzumab-conjugated polyurethanes maintain excellent micellization performance, with the size and zeta potential increasing slightly and the morphology and drug loading capacity of PM nearly unchanged. Importantly, trastuzumab has a great influence on the internalization mechanism of micelles by SKOV-3 tumor cells. We found that the PM are mainly internalized *via* micropinocytosis, and the uptake of trastuzumab-conjugated TPM by SKOV-3 cells primarily occurred *via* a clathrin-mediated endocytosis, a classic receptor-mediated endocytosis, indicating that the trastuzumab could trigger the receptor-mediated endocytosis after the combination to HER2 when conjugated to PM. Particularly, the receptor-mediated endocytosis of TPM caused more efficient cell entry and enhanced anticancer efficacy of chemotherapeutic drugs both *in vitro* and *in vivo*. This study provided strong evidence for the understanding of the acting mechanism of trastuzumab, and provided an effective strategy for the design and development of new multifunctional BDSs for cancer therapy.

REFERENCES

1 Hanahan, D. and Weinberg, R., Cell, 2011, 144(5): 646

2 Holohan, C., van Schaeybroeck, S., Longley, D.B. and Johnston, P.G., Nat. Rev. Cancer., 2013, 13(10): 714

3 Yachida, S., Jones, S., Bozic, I., Antal, T., Leary, R., Fu, B., Kamiyama, M., Hruban, R.H., Eshleman, J.R. and Nowak, M.A., Nature, 2010, 467(7319): 1114

4 Vogelstein, B., Papadopoulos, N., Velculescu, V.E., Zhou, S., Diaz, L.A. and Kinzler, K.W., Science, 2013, 339(6127): 1546
5 Shi, J., Kantoff, P.W., Wooster, R. and Farokhzad, O.C., Nat. Rev. Cancer, 2017, 17(1): 20
6 Gu, L. and Mooney, D.J., Nat. Rev. Cancer, 2015, 16(1): 56
7 Saleh, T. and Shojaosadati, S.A., Hum. Vacc. Immunother., 2016, 12(7): 1863
8 Asadi, N., Davaran, S., Panahi, Y., Hasanzadeh, A., Malakootikhah, J., Fallah, Moafi, H. and Akbarzadeh, A., Artif. Cell Nanomed. Biotechnol., 2017, 45(1): 18
9 Zheng, Y., Stephan, M.T., Gai, S.A., Abraham, W., Shearer, A. and Irvine, D.J., J. Control. Release, 2011, 172(2): 426
10 Noh, Y.W., Kim, S.Y., Kim, J.E., Kim, S., Ryu, J., Kim, I., Lee, E., Um, S.H. and Lim, Y.T., Adv. Funct. Mater., 2017, DOI: 10.1002/adfm.201605398
11 Koshy, S.T., Cheung, A.S., Gu, L., Graveline, A.R., and Mooney, D.J., Adv. Biosys., 2017, (1): 1600013
12 Lv, S., Li, M., Tang, Z., Song, W., Sun, H., Liu, H. and Chen, X., Acta Biomater., 2013, 9(12): 9330
13 Torchilin V.P., Nat. Rev. Drug Discov., 2014, 13(11): 813
14 Yoo, J.W., Chambers, E. and Mitragotri, S., Curr. Pharm. Design., 2010, 16(21): 2298
15 Petros, R.A. and Desimone, J.M., Nat. Rev. Drug. Discov., 2010, 9(9): 615
16 Bertrand, N., Wu, J., Xu, X., Kamaly, N. and Farokhzad, O.C., Adv. Drug. Deliver. Rev., 2014, 66(1): 2
17 Bazak, R., Houri, M., El Achy, S., Kamel, S. and Refaat, T., J. Cancer Res. Clin. Oncol., 2015, 141(5): 769
18 Mura, S., Nicolas, J. and Couvreur, P., Nat. Mater., 2013, 12(11): 991
19 Lu, D., Wen, X., Liang, J., Zhang, X., Gu, Z. and Fan, Y., Chinese J. Polym. Sci., 2008, 26(3): 369
20 Yu. S., Ding. J., He, C., Cao, Y., Xu, W. and Chen, X., Adv. Health. Mater., 2014, 3(5): 752
21 Xu, S., Olenyuk, B.Z., Okamoto, C.T. and Hamm-Alvarez, S.F., Adv. Drug. Deliver. Rev., 2013, 65(1): 121
22 Xu, C., Sui, M., Tang, J. and Shen, Y., Chinese J. Polym. Sci., 2011, 29(3): 274
23 Gao, C., Wang, Y., Zhu, W. and Shen, Z., Chinese J. Polym. Sci., 2014, 32(11): 1431
24 Karimi, M., Ghasemi, A., Zangabad, P.S., Rahighi, R., Basri, S.M.M., Mirshekari, H., Amiri, M., Pishabad, Z.S., Aslani, A., Bozorgomid, M., Ghosh, D., Beyzavi, A., Vaseghi, A., Aref, A.R., Haghani, L., Bahrami, S., Hamblin, M.R., Chem. Soc. Rev., 2016, 45(5): 1457
25 Byrne, J.D., Betancourt, T. and Brannon-Peppas, L., Adv. Drug. Deliver. Rev., 2008, 60(15): 1615
26 Torchilin V.P., "Drug delivery" (in English), Springer Berlin Heidelberg, Berlin Heidelberg, 2010, p. 3
27 Song, H., He, R., Wang, K., Jing, R., Bao, C., Li, N., Ji, J. and Cui, D., Biomaterials, 2010, 31(8): 2302
28 He, C., Tang, Z., Tian, H. and Chen, X., Adv. Drug. Deliver. Rev., 2016, 98(1): 64
29 Wu, X., Chen, J., Wu, M. and Zhao, J.X., Theranostics, 2015, 5(4): 322
30 Zhu, H., Li, J., Zhang, X.B., Ye, M. and Tan, W., ChemMedChem., 2015, 10(1): 39
31 Shuhendler, A.J., Prasad, P., Leung, M., Rauth, A.M., Dacosta, R.S. and Xiao, Y.W., Adv. Healthc. Mater., 2012, 1(5): 600
32 Sun, X., Xu, J., Tang, J., Sui, M. and Shen, Y., Chinese J. Polym. Sci., 2011, 29(4): 427
33 Baselga, J. and Albanell, J., J. Ann. Oncol., 2001, 12(Suppl): S35
34 Cameron, D.A. and Stein, S., Nat. Clin. Pract. Oncol., 2008, 5(9): 512
35 Nahta, R., Yu, D. and Hung, M.C., Nat. Clin. Pract. Oncol., 2006, 3(5): 269
36 Tai, W., Mahato, R., Cheng, K., J. Control. Release, 2010, 146(146): 264
37 Press, M.F., Cordon-Cardo, C. and Slamon, D.J., Oncogene, 1990, 5(7): 953
38 Germershaus, O. and Bakowsky, M.U., Bioconjugate Chem., 2006, 17(5): 1190
39 Liu, Y., Li, K., Liu, B. and Feng, S.S., Biomaterials, 2010, 31(35): 9145
40 Sun, B., Ranganathan, B. and Feng, S., Biomaterials, 2008, 29(4): 475
41 Hillaireau, H. and Couvreur, P., Cell. Mol. Life. Sci., 2009, 66(17): 2873
42 Hu, X., Hu, J., Tian, J., Ge, Z., Zhang, G., Luo, K. and Liu, S., J. Am. Chem. Soc., 2013, 135(46): 17617
43 Valabrega, G., Montemurro, F. and Aglietta, M., Ann. Oncol., 2007, 18(6): 977
44 Ben-Kasus, T., Schechter, B., Lavi, S., Yarden, Y. and Sela, M., P. Natl. Acad. Sci., 2009, 106(9): 3294

45 Cuello, M., Ettenberg, S.A., Clark, A.S., Keane, M.M., Posner, R.H., Nau, M.M., Dennis, P.A. and Lipkowitz, S., Cancer Res., 2001, 61(12): 4892
46 Fiszman, G.L. and Jasnis, M.A., J. Breast Cancer, 2011, 2011: 352182
47 Hommelgaard, A.M., Lerdrup, M. and van Deurs, B., Mol. Biol. Cell., 2004, 15(4): 1557
48 Song, N., Ding, M., Pan, Z., Li, J., Zhou, L., Tan, H. and Fu, Q., Biomacromolecules, 2013, 14(12): 4407
49 Ding, M., Li, J., He, X., Song, N., Tan, H., Zhang, Y., Zhou, L., Gu, Q., Deng, H. and Fu, Q., Adv. Mater., 2012, 24(27): 3639
50 Pan, Z., Ren, Y., Song, N., Song, Y., Li, J., He, X., Luo, F., Tan, H. and Fu, Q., Biomacromolecules, 2016, 17(6): 2148
51 Ding, M., Song, N., He, X., Li, J., Zhou, L., Tan, H., Fu, Q. and Gu, Q., ACS Nano, 2013, 7(3): 1918
52 Ding, M., Li, J., Tan, H. and Fu, Q., Soft Matter, 2012, 8(20): 5414
53 Ding, M., Zeng, X., He, X., Li, J., Tan, H. and Fu, Q., Biomacromolecules, 2014, 15(8): 2896
54 Zhou, L., Liang, D., He, X., Li, J., Tan, H., Li, J., Fu, Q. and Gu, Q., Biomaterials, 2012, 33(9): 2734
55 Liu, P., Sun, Y., Wang, Q., Sun, Y., Li, H. and Duan, Y., Biomaterials, 2014, 35(2): 760
56 Agarwal, R., Singh, V., Jurney, P., Shi, L., Sreenivasan, S.V. and Roy, K., P. Natl. Acad. Sci., 2013, 110(43): 17247
57 Agus, D.B., Bunn, P.A., Franklin, W., Garcia, M. and Ozols, R.F., Semin. Oncol., 2000, 27(6 Suppl 11): 92
58 Hudis, C.A., New Engl. J. Med., 2007, 357(1): 39
59 Kobayashi, H., Watanabe, R. and Choyke, P.L., Theranostics, 2013, 4(1): 81
60 Iversen, T.G., Skotland, T. and Sandvig, K., Nano Today, 2011, 6(2): 176
61 Pelkmans, L. and Helenius, A., Science, 2002, 296(5567): 535
62 Pickl, M. and Ries, C.H., Oncogene, 2009, 28(3): 461
63 Cirstoiu-Hapca, A., Bossy-Nobs, L., Buchegger, F., Gurny, R. and Delie, F., Int. J. Pharm., 2007, 331(2): 190
64 Song, N., Zhou, L., Li, J., Pan, Z., He, X., Tan, H., Wan, X., Li, J., Ran, R. and Fu, Q., Nanoscale, 2016, 8(14): 7711
65 Liang, H.F., Chen, C.T., Chen, S.C., Kulkarni, A.R., Chiu, Y.L., Chen, M.C. and Sung, H.W., Biomaterials, 2006, 27(9): 2051
66 Alani, A.W.G., Bae, Y., Rao, D.A. and Kwon, G.S., Biomaterials, 2010, 31(7): 1765
67 Faratian, D., Zweemer, A.J., Nagumo, Y., Sims, A.H., Muir, M., Dodds, M., Mullen, P., Um, I., Kay, C., Hasmann, M., Harrison, D.J. and Langdon, S.P., Clin. Cancer Res., 2011, 17(13): 4451